Transactions of the Materials Research Society of Japan 31[4] 859-864 (2006)

Spark Plasma Sintering of Iron Powder

Hidekazu Sueyoshi [1)], Tomohito Maruno [2)], Yasushi Maeda [2)]
and Tatsuro Onomoto [3)]
1)Department of Nano Structure and Advanced Materials, Graduate School of Science and Engineering, Kagoshima University, Kagoshima, 890-0065, Japan
Fax: 81-99-285-7704, e-mail: sueyoshi@mech.kagoshima-u.ac.jp
2) Graduate Student, Kagoshima University
3) Fukuoka Industrial Technology Center, Kitakyushu, Fukuoka, 807-0831, Japan

Spark plasma sintering (SPS) behavior of pure iron powder was examined in detail. The sintering is controlled by both iron diffusion at necking region and plastic flow of the iron powder. As compaction pressure is high, plastic flow of the iron powder becomes large, resulting in a decrease in porosity and an increase in Vickers hardness of the sintered compact. High desification is obtained by SPS at the sintering temperature higher than 1173 K for 720 s under a compaction pressure of 70 MPa. This is because enhanced iron diffusion and large plastic flow are achieved under these SPS conditions. Decomposition of iron oxide film which is formed on the surface of the iron powder occurs under SPS process, resulting in refining the surface of the iron powder. Thus, it is possible to obtain a high-densification compact by SPS at a relatively low temperature (1173 K) for a short holding time (720 s) without the usual pre-treatment for reduction of oxide film
Keywords: spark plasma sintering, pure iron powder, hardness, porosity, sintering mechanism

1. INTRODUCTION

Fiber-reinforced metal is a metal-matrix composite reinforced with high-strength fiber. Because aluminum is light and has a low melting temperature, several aluminum matrix composites have been developed. Since iron has a high melting temperature, reaction at the fiber/matrix interface is activated, resulting in damage of fiber. Therefore powder metallurgy is suitable for the production process of iron-matrix composite. However, there have been few reports regarding a fiber-reinforced iron-matrix composite.

We have examined the processing of continuous ceramic fiber/iron alloy composite by hot isostatic pressing and hot pressing, and have reported that the preparation of a continuous ceramic fiber/iron alloy composite with uniform dispersion of fiber becomes feasible by choosing an appropriate combination of mixing method of fiber and iron alloy powder and sintering [1,2]. Much attention have recently been paid to spark plasma sintering (SPS) as a new sintering method. In SPS, generation of spark plasma between powder particles, activation of the surface of the powder due to spark plasma, and promotion of atom diffusion due to plasma energy may occur, resulting in decreases in the sintering temperature and time as compared with conventional sintering methods [3]. As the application of SPS to iron alloys, the results of high-Cr iron alloys [4-9], high-Cr cast iron [10-12], and Fe-0.8mass%C alloy [13] have been reported. However there have been few reports regarding the application of SPS to fiber-reinforced iron-matrix composite. In addition, activation of the surface of the iron powder with oxide film owing to spark plasma and sintering behavior of iron powder during SPS have not been well understood to date [14]. It is necessary to clear SPS behavior in order to prepare a fiber-reinforced iron-matrix composite by using SPS.

In the present study, SPS behavior of iron powder was examined in detail.

2. EXPERIMENTAL PROCEDURE

High-purity carbonyl iron powder (Mitsuwa Chemical Co., Ltd., Fe; 99.80 mass%, C; 0.01 mass%, N; <0.01 mass%, O; 0.15 mass%) having a mean particle diameter of 3.3 μ m was used. Figure 1 shows a secondary electron (SE) image of as-received iron powder. The iron powder was a nearly spherical shape. The iron powders were packed into graphite mold (inner diameter: 30 mm), followed by SPS (Sumitomo Coal Mining Co., Ltd., PAS-III) in a vacuum (9.98 Pa).

Figure 2 shows a schematic diagram of SPS process. At first, compaction was conducted under a given pressure. Thereafter pulsating current was passed for

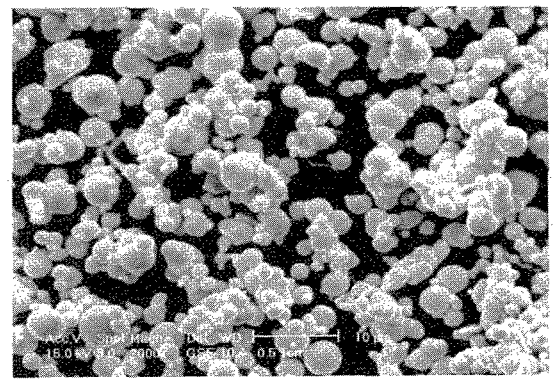

Fig. 1 SE image of as-received iron powder.

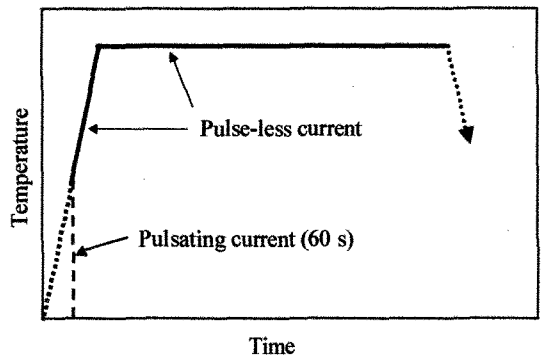

Fig. 2 Schematic diagram of SPS process.

60 s, followed by heating and holding with a pulse-less current. After holding for 720 s, the current was cut off and then the sintered compact was slowly cooled. SPS was conducted under various conditions of temperature (from 1123 to 1223 K) and compaction pressure (from 35 to 70 MPa). In order to examine a sintering shrinkage, compact length change was continuously measured during SPS by dilatometry.

We obtained a porosity of the sintered compact from the following equation:

$$P = (1 - V_0/V_s) \times 100 \quad \% \qquad (1)$$

where P is the porosity, V_0 is the theoretical volume (P = 0 %) obtained by dividing the mass of the sintered compact by the density of iron, and V_s is the measured volume of the sintered compact.

In order to examine the effect of SPS on the iron oxide film formed on the surface of the iron powder, X-ray photoelectron spectroscopy (XPS) (Shimadzu Co. Ltd., ESCA-1000) analyses of as-received powder, the powder which was passed pulsating current for 60 s, and the sintered compact were carried out, respectively.

Microstructure of the cross section of the sintered compact was examined using a scanning electron microscopy. Vickers hardness (Shimadzu Co. Ltd., HMV-1/2) of the cross section of the sintered compact was measured along radial and axial directions under a load of 0.97 N.

3. RESULTS AND DISCUSSION

Figure 3 shows SE images of the center of the cross section in the sintered compact prepared by sintering at 1173 K. A few pores (black part) appeared in the case of low compaction pressure (35 MPa). As compaction pressure was high (70 MPa), the pores decreased considerably as shown in Fig. 3(b).

Figure 4 shows the changes in Vickers hardness of the center of the cross section and porosity in the sintered compact with compaction pressure for SPS conducted at 1173 K. The porosity decreased abruptly with increasing compaction pressure. On the other hand, Vickers hardness showed inverse relation that it increased with increasing compaction pressure.

Figure 5 shows the changes in Vickers hardness of the center of the cross section and porosity in the sintered compact with sintering temperature for SPS

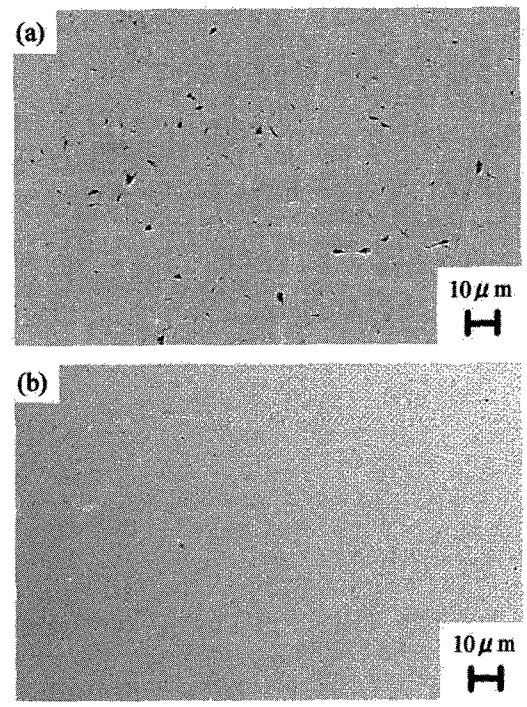

Fig. 3 SE images of the center of the cross section in the sintered compact prepared by sintering at 1173 K. (a) compaction pressure: 35 MPa, and (b) compaction pressure: 70 MPa

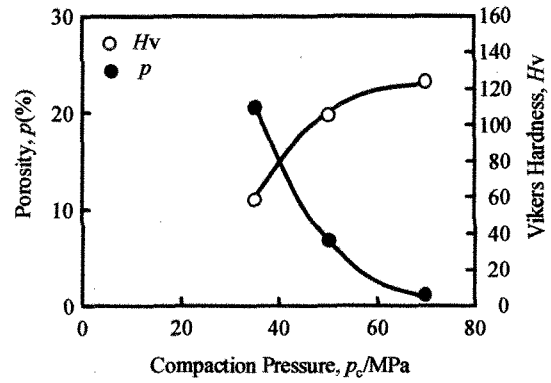

Fig. 4 Changes in Vickers hardness of the center of the cross section and porosity in the sintered compact with compaction pressure.

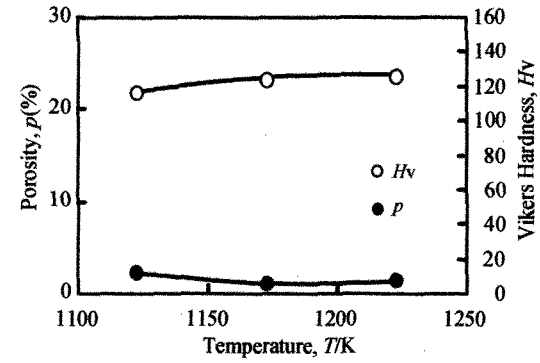

Fig. 5 Changes in Vickers hardness of the center of the cross section and porosity in the sintered compact with sintering temperature.

conducted under the compaction pressure of 70 MPa. The sintered compact having highVickers hardness and low porosity was achieved in the temperature range higher than 1173 K.

Figure 6 shows a relationship between Vickers hardness and porosity. Vickers hardness increased with decreasing porosity.

Figure 7 shows Vickers hardness distribution along radial and axial directions of the cross section of the sintered compact. As shown in Fig. 7(a), Vickers hardness along radial direction was nearly constant from the surface to the center. On the other hand, Vickers hardness along axial direction (Fig. 7(b)) increased only slightly near the surface. Using SPS, it is possible to obtain a homogeneous compact in which Vickers hardness and porosity are almost constant from the surface to the center.

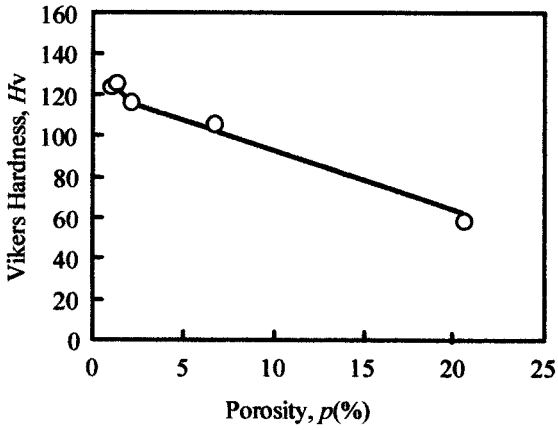

Fig. 6 Relationship between Vickers hardness and porosity.

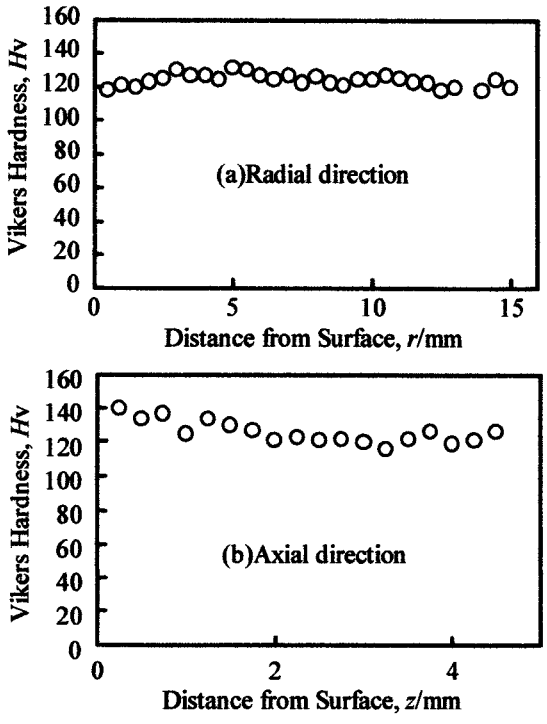

Fig. 7 Vickers hardness distribution of the cross section of the sintered compact. (a) radial direction, and (b) axial direction.

In solid state sintering, shrinkage during initial stage sintering is expressed as follows [15]:

$$(\Delta L/L_0)^{n/2} = Bt/2^n d^m \qquad (2)$$

where the shrinkage $\Delta L/L_0$ is the compact length change (ΔL) divided by the initial length (L_0), t is the isothermal sintering time (holding time), d is the particle diameter of the powder, and n and m are the constants. The parameter B is exponentially dependent on temperature:

$$B = B_0 \exp(-Q/kT) \qquad (3)$$

where B_0 is material parameter regarding surface energy, atomic size, atomic vibration frequency, and system geometry, Q is activation energy, k is the Boltzmann constant, and T is sintering temperature. Talking the logarithm of the both sides of eq. (2) yields

$$\log(\Delta L/L_0) = 2/n \cdot \log t + 2/n \cdot \log(B/2^n d^m) \qquad (4)$$

Equation (4) shows that a linear relationship exists between $\log(\Delta L/L_0)$ and $\log t$. In the SPS machine used in the present study, passing the current was allowed only after compaction pressure was applied. Under a compaction pressure of 70 MPa, the compact length decreased with increasing time until the temperature reachs to the given sintering temperature, but thereafter the compact length remained unchanged by holding time. Figure 8 shows a relationship between $\log(\Delta L/L_0)$ and $\log t$ under a compaction pressure of 35 MPa. A linear relationship held. We obtained $n = 3.57$ from a slop of the straight line in Fig. 8. Many experiments have been analyzed using n to identify the sintering mechanism. The values of n are give as follows: viscous flow; 2, plastic flow; 2, evaporation-condensation; 3, volume diffusion; 5, grain boundary diffusion; 6, surface diffusion; 7 [15]. In SPS condition used in this study, evaporation-condensation mechanism may be impractical. The result of $n = 3.57$ imply that the sintering is controlled by both diffusion of iron atom at necking region and plastic flow of the iron powder.

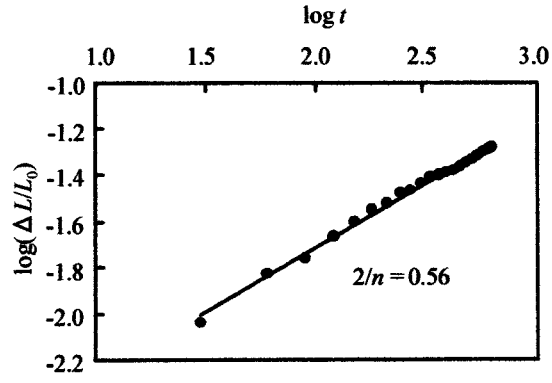

Fig. 8 Relationship between $\log(\Delta L/L_0)$ and $\log t$ under a compaction pressure of 35 MPa.

As compaction pressure is high, plastic flow of the iron powder becomes large. The result that the porosity in the sintered compact decreases abruptly with increasing compaction pressure, as shown in Fig. 4, is thought to be due to plastic flow of the iron powder.

We can roughly estimate diffusion distance by the following equation [16]:

$$x = (Dt)^{1/2} \quad (5)$$

where x is diffusion distance and D is diffusivity. D is expressed as

$$D = D_0 \exp(-Q_D/RT) \quad (6)$$

where D_o is the frequency factor, Q_D is the activation energy for diffusion of iron, and R is the gas constant. Substituting D_0=2.0 cm^2/s and Q_D= 240 kJ/mol for volume diffusion in α Fe, D_0=0.49 cm^2/s and Q_D= 284 kJ/mol for volume diffusion in γ Fe [17], and R = 8.31 J/(mol·K) into eqs. (5) and (6), we obtained Fig. 9. It is found from Fig. 9 that diffusion distance in α Fe (1123 K and 1173 K) is larger than that in γ Fe (1223 K). It is well known that the rate of grain boundary diffusion is larger than that of volume diffusion. Therefore, it is thought that each diffusion distance after 720 s is sufficient to achieve binding between iron powders. At a sintering temperature of 1223 K, a large plastic flow of the iron powder (γ Fe) occurs because of degradation of strength of the iron powder. On the other hand, at a sintering temperature of 1123 K, the plastic flow becomes low because the strength of the iron powder (α Fe) is relatively high at this temperature. The plastic flow at a temperature of 1173 K is higher than that at 1123 K. Thus, iron diffusion behavior at necking region and plastic flow of the iron powder influence the densification. The result (Fig. 5) that the porosity of the sintered compact was low and also was almost independent of the sintering temperature in the temperature range higher than 1173 K is cause by the behavior mentioned above.

Figure 10 shows the XPS spectra of as-received iron powder. In Fe2p spectrum near the surface (8 nm from the surface), clear peaks of metallic iron (2p3/2: 706.75 eV, 2p1/2: 719.95 eV) were not detected, while the peaks of Fe_2O_3 (2p3/2: 710.7 eV, 2p1/2: 724.3 eV) were observed clearly. And also in O1s spectra the peak of Fe_2O_3 (530 eV) was clearly detected. In the XPS spectra after etching, a well-defined peaks of metallic iron appeared. Also, the intensities of the peaks of metallic iron increased with increasing depth from the surface. From Fig. 10, the thickness of iron oxide film seems to be several ten nm.

Figure 11 shows the XPS spectra of the iron powder after passing a pulsating current for 60 s. These spectra were similar to those shown in Fig. 10. This suggests that incomplete decomposition of iron oxide film was achieved by passing a pulsating current for 60 s.

Figure 12 shows the XPS spectra of the center of the cross section in the sintered compact prepared by sintering at 1173 K under a compaction pressure of 70 MPa. Although, the peak of iron oxide appeared slightly in O1s spectra, the peak of iron oxide was not evidently as compared with the defined peak of metallic iron. This suggests that the decomposition of iron oxide film occured during passing not only pulsating current but also pulse-less current. This is because discharge of plasma and decomposition of iron oxide film occur with an enormous Joule heat generation at particle contact region at which a high current density is achieved. As mentioned above, it was possible to obtain

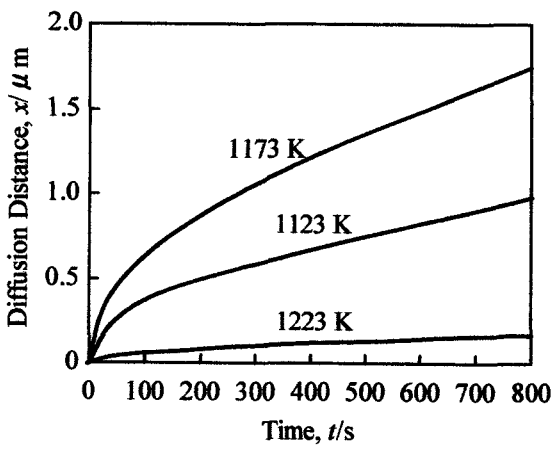

Fig. 9 Relationship between x and t.

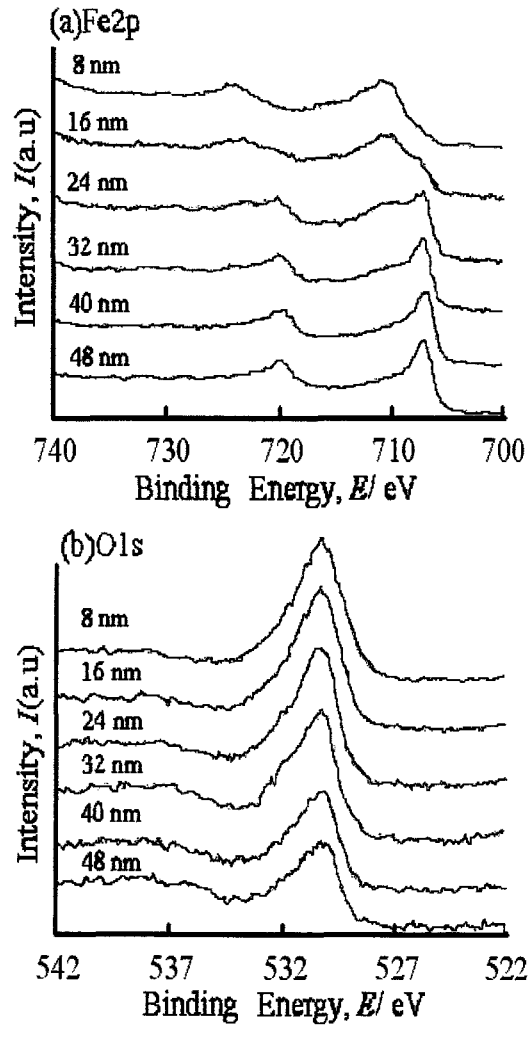

Fig. 10 XPS spectra of as-received iron powder.

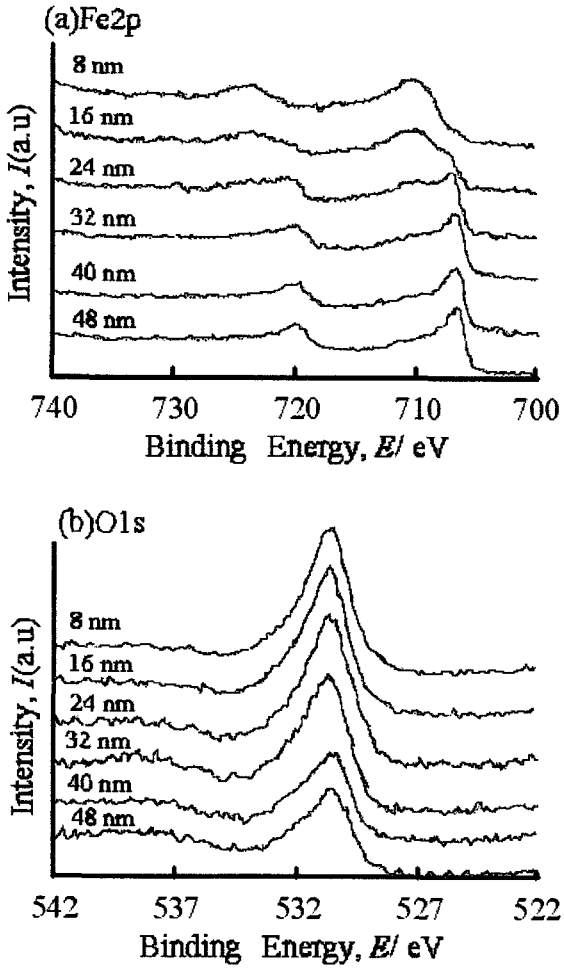

Fig. 11 XPS spectra of the iron powder after passing a pulsating current for 60 s.

a high densification compact by SPS at relatively low temperature (1173 K). This is because decomposition of iron oxide film occurs during SPS, resulting in refining the surface of the iron powder. Thus, in LIPS it is unnecessary to perform the usual pre-treatment for reduction of oxide film of the iron powder.

4. CONCLUSIONS

From the results of SPS of pure iron powder, the following conclusions were obtained.

(1)The sintering is controlled by both iron diffusion at necking region and plastic flow of the iron powder.

(2)As compaction pressure is high, plastic flow of the iron powder becomes large, resulting in a decrease in porosity and an increase in Vickers hardness of the sintered compact.

(3) High desification is obtained by SPS at the sintering temperature higher than 1173 K for 720 s under a compaction pressure of 70 MPa. This is because enhanced iron diffusion and large plastic flow are achieved under these SPS conditions.

(4)Decomposition of iron oxide film formed on the surface of the iron powder occurs under SPS process, resulting in refining the surface of the iron powder.

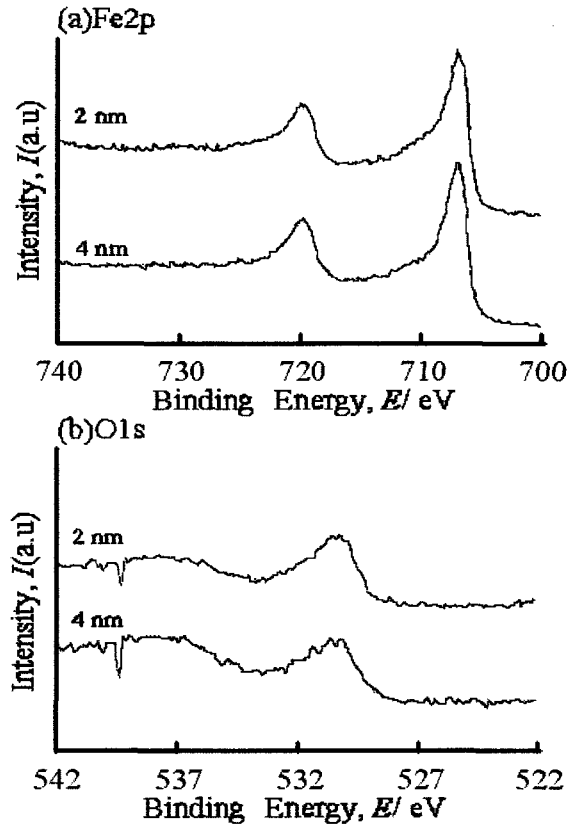

Fig. 12 XPS spectra of the center of the cross section of the sintered compact.

Thus, it is possible to obtain a high-densification compact by SPS at a relatively low temperature (1173 K) for a short holding time (720 s) without the usual pre-treatment for reduction of oxide film.

REFERENCES

1)H. Sueyoshi, T. Maruno, K. Yamamoto, Y. Hirata, S. Sameshima, S. Uchida, S. Hamauzu and S. Kurita, *Materials Trans.*, 43, 735-740 (2002).

2)H. Sueyoshi, T.Maruno, M. Asano, Y. Hirata, S. Sameshima, S. Uchida, S. Hamauzu and S. Kurita, *Materials Trans.*, 43, 2866-2872 (2002).

3)M. Tokita, *J. High Temperature Society*, 31, 215-224 (2005).

4)N. Matsui, K. Kobayashi, A. Sugiyama and K. Ozaki, *J. Japan Society of Powder and Powder Metallurgy*, 44, 1121-1125 (1997).

5) N. Matsui, K. Kobayashi, A. Sugiyama and K. Ozaki, *J. Japan Society of Powder and Powder Metallurgy*, 45, 1081-1085 (1998).

6) N. Matsui, K. Matsui, K. Kobayashi, A. Sugiyama and K. Ozaki, *J. Japan Society of Powder and Powder Metallurgy*, 46, 1179-1184 (1999).

7) N. Matsui, K. Matsui, K. Kobayashi, A. Sugiyama and K. Ozaki, *J. Japan Society of Powder and Powder Metallurgy*, 47, 30-35 (2000).

8) N. Matsui, T. Yamada, K. Kobayashi, A. Sugiyama and K. Ozaki, *J. Japan Society of Powder and Powder Metallurgy*, 47, 332-336 (2000).

(Received September 5, 2006;Accepted November 15, 2006)

9) K. Kobayashi, A. Matsumoto, T. Nishio, K. Ozaki and A. Sugiyama, *J. Japan Society of Powder and Powder Metallurgy*, 47, 1097-1101 (2000).
10)T. Satoh, M. Sakamoto and H. N. Liu, *J. Japan Society of Powder and Powder Metallurgy*,48, 1119-1125 (2001).
11)T. Satoh, H. N. Liu, M. Sakamoto, Y. Kawakami and K. Ogi, *J. Japan Society of Powder and Powder Metallurgy*, 50, 963-967 (2003).
12) T. Satoh, H. N. Liu, M. Sakamoto and Y. Kawakami, *J. Materials Science*, 40, 3283-3286 (2005).
13)H. W. Zhang, R. Gopalan, T. Mukai and K. Hono, *Scripta Materialia*, 53, 863-868 (2005).
14)K. Ozaki, *J. High Temperature Society*, 31, 209-214 (2005).
15)ASM International, "ASM Handbook Vol.7 Powder Metal Technologies and Applications", ASM International, Ohio (1998) pp.449-452.
16)P. G. Shewmon, " Diffusion in Solids ", McGraw -Hill, London (1963) p.6.
17)Japan Inst. Metals, "A Data Book on Metals", Maruzen, Tokyo (1974) p.25.

(Received September 5, 2006;Accepted November 15, 2006)